
[View Journal Online](#)
[View Article Online](#)

Synthesis, crystal structure, DFT and Hirshfeld surface analysis of 4-fluoro-*N*-(1,3-dioxoisindolin-2-yl)benzamide

Ramakrishnan Elancheran *, Balakrishnan Karthikeyan , Subramanian Srinivasan ,
 Kuppusamy Krishnasamy  and Senthamaraikannan Kabilan *

Department of Chemistry, Annamalai University, Chidambaram-608002, Tamil Nadu, India

* Corresponding author at: Department of Chemistry, Annamalai University, Chidambaram-608002, Tamil Nadu, India.
 e-mail: srielancheran@gmail.com (R. Elancheran), profdrskabilanau@gmail.com (S. Kabilan).

RESEARCH ARTICLE

ABSTRACT



doi 10.5155/eurjchem.14.1.1-8.2335

Received: 15 August 2022

Received in revised form: 10 November 2022

Accepted: 15 November 2022

Published online: 31 March 2023

Printed: 31 March 2023

KEYWORDS

DFT
 Synthesis
 Benzamide
 Single crystal XRD
 HOMO/LUMO energies
 Hirshfeld surface analysis

The 4-fluoro-*N*-(1,3-dioxoisindolin-2-yl)benzamide was synthesized by the reaction of 4-fluorobenzohydrazide with phthalic anhydride in acetic acid. The compound was characterized by analytical instruments like FT-IR and NMR. The three-dimensional structure of the title compound was further confirmed by single-crystal X-ray diffraction study. In addition to the experimental study, theoretical calculations were performed to explore the molecular structure in order to analyze experimental and theoretical findings. The title compound crystallizes in the monoclinic space group $P2_1/n$ as determined by the X-ray diffraction investigation, crystal data for $C_{15}H_9FN_2O_3 \cdot H_2O$: $a = 14.094(6)$ Å, $b = 7.248(3)$ Å, $c = 14.517(6)$ Å, $\beta = 105.116(14)^\circ$, $V = 1431.6(10)$ Å³, $Z = 4$, $T = 298(2)$ K, $\mu(\text{MoK}\alpha) = 0.112$ mm⁻¹, $D_{\text{calc}} = 1.402$ g/cm³, 37521 reflections measured ($4.684^\circ \leq 2\theta \leq 60.6^\circ$), 4225 unique ($R_{\text{int}} = 0.0517$, $R_{\text{sigma}} = 0.0311$) that were used in all calculations. The final R_1 was 0.0537 ($I > 2\sigma(I)$) and wR_2 was 0.1501 (all data). The N-H...O and O-H...O hydrogen bonds linking molecules in the crystal form a three-dimensional framework structure. The electronic states and molecular properties of the title compound were determined using computational studies, like density functional theory and Hirshfeld surface analysis.

Cite this: *Eur. J. Chem.* 2023, 14(1), 1-8

Journal website: www.eurjchem.com

1. Introduction

The 4-fluorobenzamide group has a wide range of pharmacological properties, including anti-inflammatory [1], analgesic [1], anticancer [2], and antidiabetic activities [3], and are also well known for having significant bioactive frameworks. Similarly, isoindoline derivatives exhibit anti-inflammatory [4], anticancer [5-7], antiviral [8,9], antibacterial [9], anti-Alzheimer's agents [10], and anticonvulsant activities [11]. It has been used in Structure Activity Relationship (SAR) investigations [12] and as a potential material for Organic Light-Emitting Diode (OLED) to substitute isoindolines with carboxylic acid groups. The carbamide group has anticonvulsant [13], antidepressant [13], and anti-human immunodeficiency virus (HIV) activities [14]. The title compound, 4-fluoro-*N*-(1,3-dioxoisindolin-2-yl)benzamide, was investigated as part of our ongoing research on derivatives of acetamide and isoindoline [15,16]. The isoindoline and 4-fluorobenzamide moieties are present in the chemical structure of 4-fluoro-*N*-(1,3-dioxoisindolin-2-yl)benzamide which was synthesized and the pure crystalline compound obtained was analyzed using FT-IR, ¹H NMR, and ¹³C NMR spectroscopic techniques. The crystal structure of 4-fluoro-*N*-(1,3-dioxoisindolin-2-yl)benzamide was acquired using a single-crystal X-ray diffractometer.

Theoretical calculations, including DFT and Hirshfeld surface analysis, were also used to obtain molecular surfaces and optimum geometry of the structure, and contacts involved in the packing of the crystals.

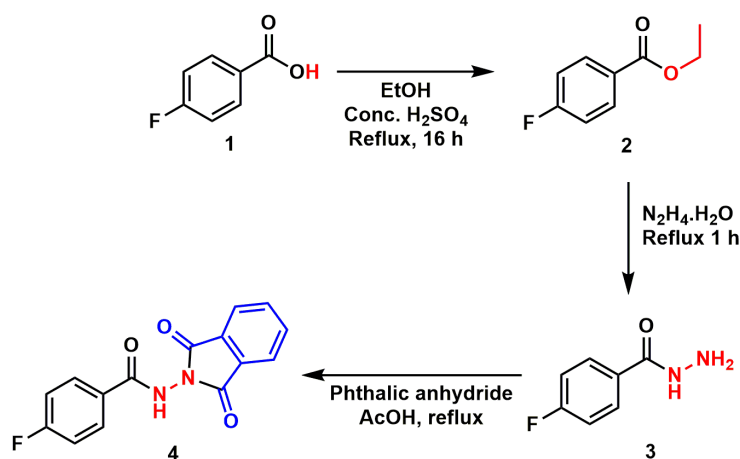
2. Experimental

2.1. General

Without further purification, all of the reagents and solvents were used after purchasing them from Sigma-Aldrich. Merck silica gel 60F₂₅₄ precoated aluminum plates were used for the thin layer chromatography (TLC) analysis, which was used to monitor the reaction. On a Thermo Nicolet FT-IR Model iS5 spectrophotometer, KBr discs were used to record FT-IR (Fourier transform infrared) spectra in cm⁻¹. Using a Bruker 400 MHz Nuclear Magnetic Resonance (NMR) instrument, ¹H and ¹³C NMR spectra were captured in CDCl₃. The chemical shift (δ) values are given in parts per million (ppm) with tetramethyl silane as the internal standard. Peak multiplicities are expressed using the following symbols: s, singlet; d, doublet; t, triplet; q, quartet; dd, doublet of doublet; br, broad; br s, broad singlet; m, multiplet.

Table 1. Crystal data and details of the structure refinement for compound 4.

Parameters	Compound 4
Empirical formula	C ₁₅ H ₉ FN ₂ O ₃ ·H ₂ O
Formula weight (g/mol)	302.26
Temperature (K)	298(2)
Crystal system	Monoclinic
Space group	<i>P</i> 2 ₁ / <i>n</i>
<i>a</i> , (Å)	14.094(6)
<i>b</i> , (Å)	7.248(3)
<i>c</i> , (Å)	14.517(6)
β (°)	105.116(14)
Volume (Å ³)	1431.6(10)
<i>Z</i>	4
ρ _{calc} (g/cm ³)	1.402
μ (mm ⁻¹)	0.112
F(000)	624.0
Crystal size (mm ³)	0.31 × 0.27 × 0.19
Radiation	MoKα (λ = 0.71073)
2θ range for data collection (°)	4.684 to 60.6
Index ranges	-19 ≤ <i>h</i> ≤ 19, -10 ≤ <i>k</i> ≤ 10, -20 ≤ <i>l</i> ≤ 20
Reflections collected	37521
Independent reflections	4225 [R _{int} = 0.0517, R _{sigma} = 0.0311]
Data/restraints/parameters	4225/0/207
Goodness-of-fit on F ²	1.045
Final R indexes [I ≥ 2σ (I)]	R ₁ = 0.0537, wR ₂ = 0.1239
Final R indexes [all data]	R ₁ = 0.1072, wR ₂ = 0.1501
Largest diff. peak/hole (e.Å ⁻³)	0.14/-0.14

**Scheme 1.** Synthesis of 4-fluoro-*N*-(1,3-dioxoisindolin-2-yl)benzamide (4).

2.2. Synthesis

To a solution of 4-fluorobenzoic acid (1 mmol) in ethanol (15 mL), a catalytic amount (3 mL) of concentrated H₂SO₄ was gradually added at room temperature, which was then refluxed for 16 hours while stirred. After the mixture was cooled, the ethanol was removed and the mixture was concentrated in a vacuum. The reaction mixture was diluted with ethyl acetate (30 mL) and then washed with saturated NaHCO₃ and cold water, followed by separating the organic layer. The mixed organic layer was brine-washed, dried over anhydrous Na₂SO₄, concentrated, and vacuum-dried for 12 hours. Ethyl 4-fluorobenzoate (1 mmol) was refluxed with hydrazine hydrate (2 mL) for one hour. Upon completion of the reaction, the reaction mixture was quenched with water and extracted with ethyl acetate. The combined organic layer was washed with a brine solution, dried over anhydrous sodium sulfate, filtered, and concentrated under reduced pressure [17]. Subsequently, phthalic anhydride was added to a 4-fluorobenzohydrazide solution in acetic acid and refluxed for 12 hours. The reaction mixture was placed over the crushed ice once the reaction had finished, as determined by TLC. To obtain the pure product, the precipitate from the ethanol was filtered, dried and recrystallized from the chloroform and methanol solvent mixture (1:1 ratio) (Scheme 1).

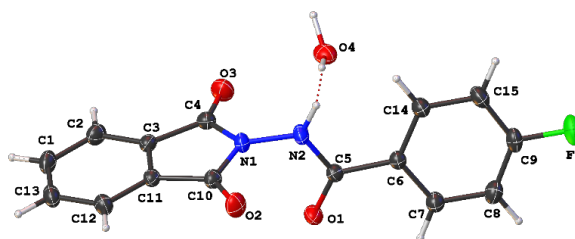
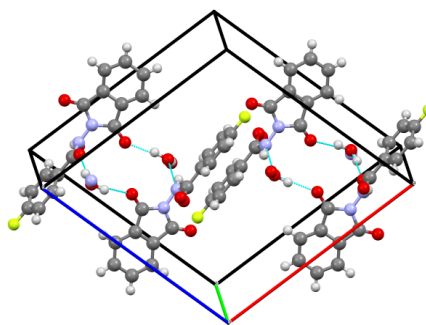
4-Fluoro-*N*-(1,3-dioxoisindolin-2-yl)benzamide (4): FT-IR (KBr, ν, cm⁻¹): 3078, 2982, 2822 (Ar. CH_{str.}), 1670 (-CO-NH_{str.}), 1600 (NH_{bend}), 1508, 1423 (C=C_{arom}), 1312, 1289, 1224 (C-H_{bend}). ¹H NMR (400 MHz, DMSO-*d*₆, δ, ppm): 8.08-8.05 (m, 4H, Ar-H), 7.98-7.93 (m, 4H, Ar-H), 7.31 (s, 1H, NH). ¹³C NMR (100 MHz, DMSO-*d*₆ & CDCl₃, δ, ppm): 170.3 (C=O), 168.7 (NH-C=O), 157.9 (C-F), 140.6 (C-Ar), 135.8 (C-Ar), 134.7 (C-Ar), 131.1 (C-Ar), 129.4 (C-Ar), 121.3 (C-Ar). HRMS (ESI, *m/z*) calculated C₁₅H₉FN₂O₃: 284.05972; [M-H]⁻; Found: 283.26868.

2.3. X-ray structure determination

On a Bruker D8 Quest diffractometer, a single-crystal X-ray diffraction (SC-XRD) experiment was carried out to determine the structure of 4-fluoro-*N*-(1,3-dioxoisindolin-2-yl)benzamide. A proper crystal was mounted onto a micro loop using Fomblin oil. MoKα radiation (λ = 0.71073 Å) was used in this study. Omega and phi-scan modes were used to record the intensities at different diffraction angles. SC-XRD data were collected at room temperature. The data was collected using APEX3 software and APEX3 was also used to index reflection data and obtain unit cell parameters [18,19]. The crystal and structure refinement data are presented in Table 1.

Table 2. Experimental and theoretical bond lengths of compound 4.

Bond	Bond lengths (Å)		Bond	Bond lengths (Å)	
	XRD	DFT (B3LYP/6-311G(d,p))		XRD	DFT (B3LYP/6-311G(d,p))
F1-C9	1.360(2)	1.39790	C3-C11	1.378(2)	1.40350
O1-C5	1.2182(19)	1.24311	C5-C6	1.482(2)	1.48736
O2-C10	1.202(2)	1.23057	C6-C7	1.380(2)	1.40395
O3-C4	1.190(2)	1.23075	C6-C14	1.376(2)	1.40472
N1-N2	1.3759(19)	1.37511	C7-C8	1.373(3)	1.39282
N1-C4	1.400(2)	1.42357	C8-C9	1.343(3)	1.38819
N1-C10	1.377(2)	1.42434	C9-C15	1.357(3)	1.38679
N2-C5	1.351(2)	1.39032	C10-C11	1.481(2)	1.48283
C1-C2	1.381(3)	1.40296	C11-C12	1.371(2)	1.38688
C1-C13	1.358(3)	1.40105	C12-C13	1.384(3)	1.40300
C2-C3	1.377(2)	1.38689	C14-C15	1.385(3)	1.39561
C3-C4	1.476(2)	1.48309			

**Figure 1.** The ORTEP diagram of compound 4 showing the atom-labeling scheme.**Figure 2.** Intermolecular H-bonding interactions of compound 4.

2.4. Computational methodology

The optimized structure was derived by quantum mechanical calculations (Gaussian 09W [20] software package, followed by the density functional group theory (DFT) B3LYP [21,22] with 6-311G(d,p) basis set). The geometric parameters obtained from the SC-XRD study were compared with those determined theoretically. The Mulliken charges, the HOMO-LUMO energy gap, and the molecular electrostatic potential (MEP) of compound 4 were calculated and they were visualized and investigated by GaussView 5.0 [23]. The CrystalExplorer3.1 program has been used to perform the Molecular Hirshfeld surfaces, fingerprint plots and crystal voids evaluation [24-26]. The contacts that are short (red), intermediate (blue), and long (white) in comparison to the sum of van der Waals interactions were shown by color coding on the d_{norm} surface. Additionally, analyses using Shape-index, curvedness, electrostatic potential, and framework analysis have been performed [24].

3. Results and discussion

3.1. Chemistry

The 4-fluorobenzohydrazide was synthesised using the commercially available 4-fluoro benzoic acid by esterification, followed by hydrazine hydrate reaction. Further, to a solution of 4-fluorobenzohydrazide in acetic acid, phthalic anhydride

was added and refluxed for 12 h. The completion of the reaction was monitored by TLC. The contents obtained were poured on crushed ice. The precipitate was filtered, dried and purified from ethanol to obtain the pure product as depicted in Scheme 1. The title compound (4) has nine protons, according to ^1H NMR analysis. Around δ 7.93 to 8.08 ppm, phenyl protons were detected as multiplets. Compound 4 includes a variety of carbon atom signals, including aromatic carbon (C=O and C-F units) according to the ^{13}C NMR results. At δ 121.3, 129.4, 131.1, 134.7, 135.8, and 140.6 ppm, aromatic carbons were observed. The presence of C=O is shown by the carbon signals at δ 168.7 and 170.3 ppm. Furthermore, FT-IR showed the appropriate absorption bands for compound 4 as well.

3.2. Crystal structure analysis

Compound 4 was crystallized under the monoclinic system with space group $P2_1/n$. The ORTEP diagram for compound 4 is shown in Figure 1. The crystallographic parameters for compound 4 are shown in Table 1. The geometrical parameters (bond length, bond angle and dihedral angle) of compound 4 are also given in Tables 2-4. Table 5 contains the details of hydrogen bonding. Furthermore, the main hydrogen bonding interactions observed in compound 4 are depicted in Figure 2. The obtained bond lengths and angles were compared with the DFT calculations and the obtained data remain within the usual limits [27,28].

Table 3. Experimental and theoretical bond angles of compound 4.

Bond	Bond angles (°)		Bond	Bond angles (°)	
	XRD	DFT (B3LYP/6-311G(d,p))		XRD	DFT (B3LYP/6-311G(d,p))
N2-N1-C4	122.60(15)	123.00	C14-C6-C7	118.25(16)	119.56
N2-N1-C10	123.93(14)	123.44	C8-C7-C	121.26(17)	120.53
C10-N1-C4	112.99(14)	112.62	C9-C8-C7	118.39(18)	118.23
C5-N2-N1	118.62(14)	119.74	C8-C9-F1	118.58(19)	118.53
C13-C1-C2	120.84(18)	120.99	C8-C9-C15	123.22(18)	123.03
C3-C2-C1	117.5(2)	117.69	C15-C9-F1	118.2(2)	118.43
C2-C3-C4	130.01(18)	129.65	O2-C10-N1	124.20(16)	125.10
C2-C3-C11	121.46(17)	121.33	O2-C10-C11	130.62(17)	130.22
C11-C3-C4	108.52(15)	109.02	N1-C10-C11	105.18(14)	104.66
O3-C4-N1	124.68(17)	125.21	C3-C11-C10	108.45(15)	109.02
O3-C4-C3	130.57(18)	130.13	C12-C11-C3	120.89(16)	121.33
N1-C4-C3	104.75(15)	104.65	C12-C11-C10	130.65(17)	129.68
O1-C5-N2	120.37(15)	121.24	C11-C12-C13	117.3(2)	117.69
O1-C5-C6	123.32(15)	123.29	C1-C13-C12	122.07(19)	120.98
N2-C5-C6	116.29(14)	115.48	C6-C14-C15	120.88(18)	120.40
C7-C6-C5	118.43(15)	117.68	C9-C15-C14	117.99(19)	118.24
C14-C6-C5	123.27(15)	122.74			

Table 4. Experimental and theoretical torsion angles of compound 4.

Bond	Torsion angles (°)		Bond	Torsion angles (°)	
	XRD	DFT (B3LYP/6-311G(d,p))		XRD	DFT (B3LYP/6-311G(d,p))
F1-C9-C15-C14	179.94(18)	-179.79	C4-N1-N2-C5	-87.5(2)	81.64
O1-C5-C6-C7	-10.9(3)	-26.51	C4-N1-C10-O2	176.38(17)	-178.54
O1-C5-C6-C14	166.49(17)	151.32	C4-N1-C10-C11	-3.42(18)	2.23
O2-C10-C11-C3	-177.48(19)	179.45	C4-C3-C11-C10	-0.46(18)	0.11
O2-C10-C11-C12	1.8(3)	-0.68	C4-C3-C11-C12	-179.78(15)	-179.77
N1-N2-C5-O1	-2.2(2)	-3.55	C5-C6-C7-C8	178.07(16)	179.41
N1-N2-C5-C6	176.44(14)	177.15	C5-C6-C14-C15	-177.44(17)	-178.98
N1-C10-C11-C3	2.30(18)	-1.38	C6-C7-C8-C9	-0.8(3)	-0.68
N1-C10-C11-C12	-178.46(17)	178.49	C6-C14-C15-C9	-0.2(3)	0.06
N2-N1-C4-O3	-4.8(3)	10.01	C7-C6-C14-C15	0.0(3)	-1.20
N2-N1-C4-C3	175.53(14)	-171.36	C7-C8-C9-F1	-179.46(17)	-179.90
N2-N1-C10-O2	4.1(3)	-9.29	C7-C8-C9-C15	0.6(3)	-0.50
N2-N1-C10-C11	-175.68(14)	171.48	C8-C9-C15-C14	-0.1(3)	0.81
N2-C5-C6-C7	170.51(16)	152.78	C10-N1-N2-C5	84.1(2)	-86.46
N2-C5-C6-C14	-12.1(2)	-29.41	C10-N1-C4-O3	-177.14(18)	179.21
C1-C2-C3-C4	179.18(18)	179.93	C10-N1-C4-C3	3.15(18)	-2.17
C1-C2-C3-C11	-0.3(3)	0.19	C10-C11-C12-C13	-178.58(17)	179.95
C2-C1-C13-C12	0.0(3)	0.04	C11-C3-C4-O3	178.79(19)	179.73
C2-C3-C4-O3	-0.7(3)	-0.04	C11-C3-C4-N1	-1.53(18)	1.20
C2-C3-C4-N1	178.98(17)	-178.56	C11-C12-C13-C1	-0.4(3)	0.17
C2-C3-C11-C10	179.09(16)	179.90	C13-C1-C2-C3	0.4(3)	-0.22
C2-C3-C11-C12	-0.2(3)	0.02	C14-C6-C7-C8	0.5(3)	1.51
C3-C11-C12-C13	0.6(3)	-0.20			

Table 5. Hydrogen bond details of compound 4*.

Donor-Hydrogen...Acceptor	D...H (Å)	H...A (Å)	D...A (Å)	∠D-H...A (°)
N2-H2A...O4 ⁱⁱ	0.86	1.96	2.75	153.6
C7-H7...O4 ⁱ	0.93	2.63	3.52	159.5
C14-H14...O4 ⁱ	0.93	2.59	3.38	143.2
O4-H4...O2 ⁱⁱⁱ	0.93	1.90	2.81	167.0
O4-H3...O1 ⁱ	0.93	1.85	2.76	166.0

* Symmetry code: (i) x, -1+y, z (ii) x, y, z (iii) 1/2-x, 1/2+y, 1/2-z.

The N-H...O and O-H...O hydrogen bonds linking molecules in the crystal form a three-dimensional framework structure. The linked benzene ring is twisted relative to the almost planar phthalimide ring system, forming a dihedral angle of 76.70(7)°. The phthalimide ring is largely planar, with a maximum deviation of 0.0479 Å for N1. In the carboxy group of the phthalimide, the carbon-oxygen distances are different in bond lengths (C10-O2 = 1.206(2) and C4-O3 = 1.190(3) Å). Intermolecular hydrogen bonding between molecules of N2-H2A...O4, O4-H4...O2 and O4-H3...O1 substantially strengthens these bonds.

3.3. Theoretical calculations

DFT calculations were carried out for compound 4 at the B3LYP/6-311G(d,p) level of theory, and Figure 3 shows the optimized structure. Since the theoretical calculations are done for an isolated molecule in a gaseous phase and the experimental results are for a molecule in a solid state, a comparison of the theoretical values with the experimental ones shows that

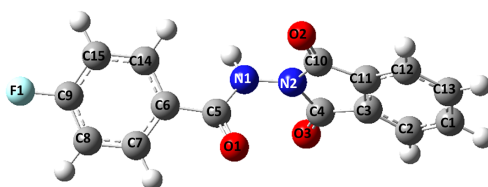
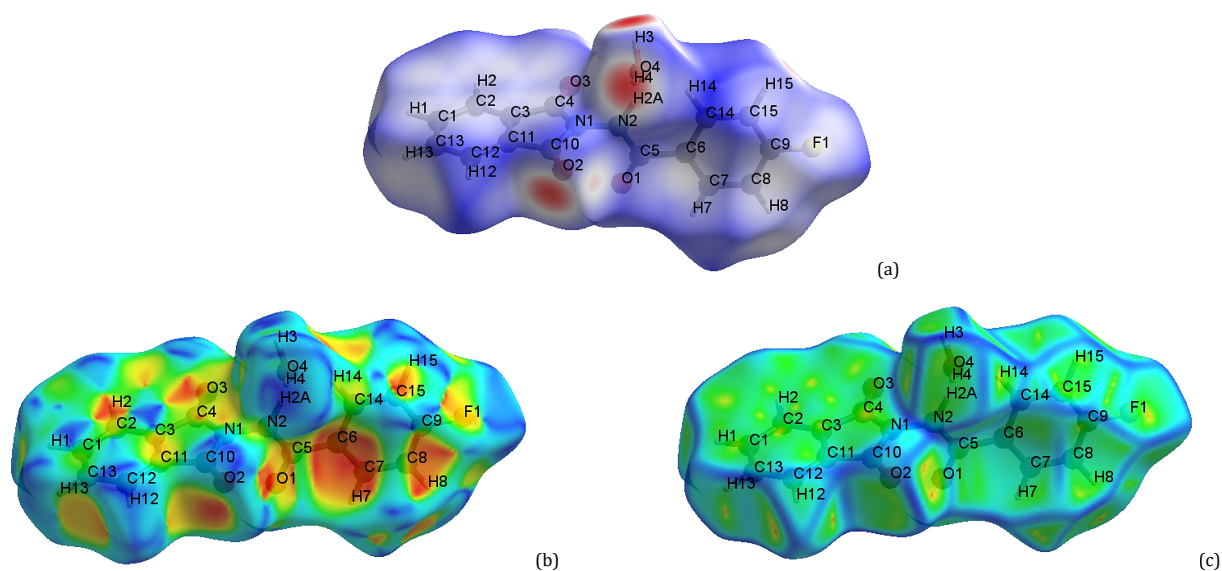
most of the optimized bond lengths are slightly larger than the experimental values (Table 2). The geometrical parameters obtained for compound 4 are given in Tables 2-4.

Hirshfeld surface analysis was obtained utilizing the CIF file from single-crystal XRD analysis to quantify and depict multiple intermolecular contacts, and they were used to explore intermolecular interactions and their quantitative contributions [29]. The region on the surface where atoms make intermolecular interactions that are closer together than the sum of their Van der Waals radii is depicted by the color red. It is notable that the Hirshfeld surface depicts the H...H bond between H2A and H4 as a red spot, indicating that this is a major short-range H...H contact. Positive electrostatic potentials are corresponding to blue zones. Neutral potentials are indicated by the white regions. The contact distances d_{norm} contain both d_i (distance from the surface to the nearest atom inside the surface) and d_e (distance from the surface to the nearest atom outside the surface) shown in Figure 4.

Table 6. Quantum chemical parameters and their values, as estimated by B3LYP/6-311G(d,p), include HOMO-LUMO energies of compound 4.

Property*	Values
E_{HOMO}	-7.4173 eV
E_{LUMO}	-2.8425 eV
$\Delta E_{LUMO-HOMO}$	4.5748 eV
Global hardness (η)	2.2874 eV
Softness (ξ)	0.2186 eV
Chemical potential (μ)	5.1299 eV
Electrophilicity (ψ)	5.5752 eV
Electronegativity (χ)	-2.2874 eV
Dipole moment (D)	4.1070 Debye

* $\eta = 1/2[E_{LUMO} - E_{HOMO}]$, $\xi = 1/2\eta$, $\mu = -[1/2(E_{LUMO} + E_{HOMO})]$, $\psi = \mu^2/2\eta$, $\chi = -\mu$.

**Figure 3.** Optimized molecular structure for compound 4.**Figure 4.** (a) d_{norm} , (b) Shape-index, and (c) Curvedness mapped on the Hirshfeld surface of compound 4.

The shape index surface in the structure of a molecule describes the surface and density of electrons surrounding a chemical interaction. The presence of C-H \cdots C $_g$ and cycle stacking (C $_g$ -C $_g$) interactions are indicated by red and blue triangles, respectively. The Hirshfeld surface of compound 4 was depicted in three dimensions in Figure 4. On the curvedness surface, the large flat region with a blue edge represents the interactions between the cycle stacking of the molecules shown in Figure 4. The fingerprint plot of compound 4 confirmed the presence of different intermolecular interactions with O \cdots H/H \cdots O (28.1%), H \cdots H (26.8%), C \cdots H/H \cdots C (25.4%), H \cdots F/F \cdots H (12.3%), C \cdots C (8.9%), C \cdots O/O \cdots C (4.7%), O \cdots F/F \cdots O (1.6%), N \cdots H/H \cdots N (1.0%). The yellowish bin on the fingerprint plots also pointed to the presence of a weak π - π stacking in the crystal structure shown in Figure 5.

The most reactive site in π -electron systems is predicted using the frontier electron density, which is also used to explain a variety of reactions in the conjugated system [30]. Higher kinetic stability and lower chemical reactivity are always correlated with higher HOMO-LUMO gaps. To remove electrons from the low-lying HOMO, it is energetically unfavorable to add an electron to the high-lying LUMO. The HOMO-LUMO energy gap (4.5748 eV) is showing good stability of the molecule shown in Figure 6. The stability, chemical activity, softness,

hardness, chemical potential, electronegativity, and electrophilicity index of a molecule are all reflected in its energy gap (E_{gap}), according to Koopman's Theorem. Table 6 shows all global reactivity values for the title compound. These parameters demonstrate that the molecule is stable when the chemical potential is negative and less reactive and more stable when the chemical hardness is high. The substance's high electrophilicity index value makes it suitable for biological action. Dipole moment arises due to the difference in electronegativity of the bonded atoms. The large magnitude of the dipole moment suggests that compound 4 may be attractive for further interactions with other systems. This typically happens when one atom has a larger electronegative value than the other atom, which allows the higher electronegative atom to pull the electron cloud more strongly.

In order to perform as the best electron donor, compound 4 ($E_{HOMO} = -7.4173$ eV) has a higher HOMO energy. In contrast, compound 4 ($E_{LUMO} = -2.8425$ eV) has a lower LUMO energy. Attributed to the importance of these two qualities, the electronegativity (χ), the electronic chemical potential (μ), and the chemical hardness (η) are so significant. In addition, it is observed that compound 4 has a dipole moment of 4.1070 Debye.

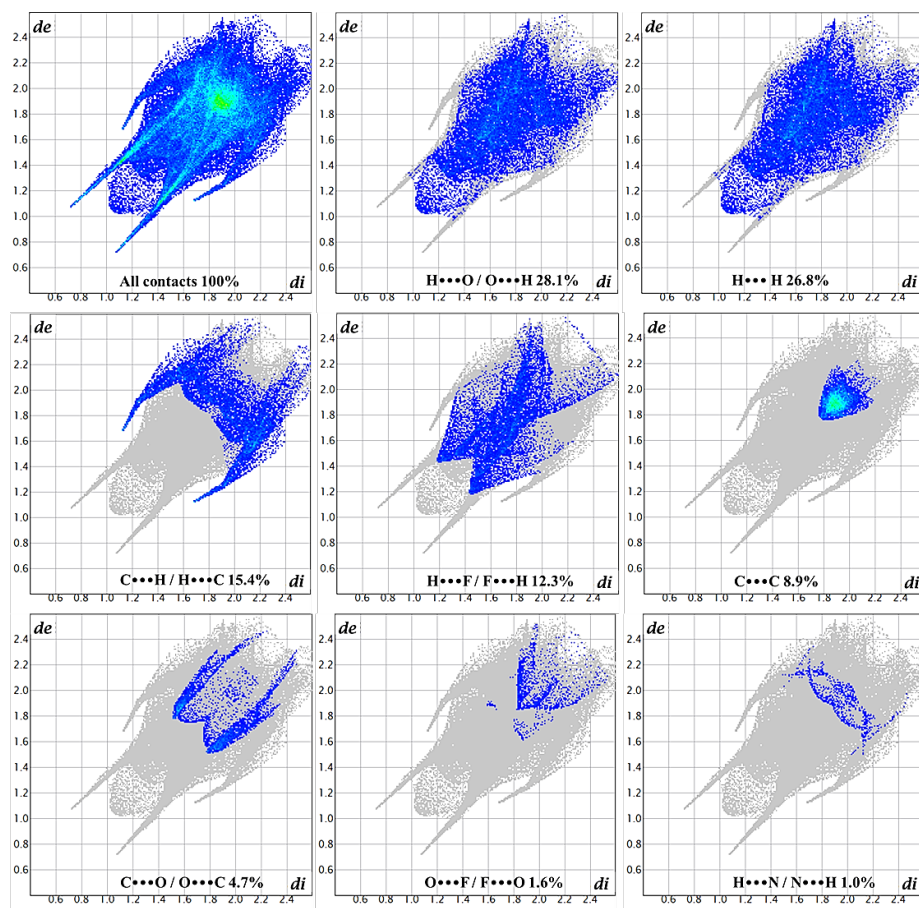


Figure 5. Fingerprint plots of compound 4.

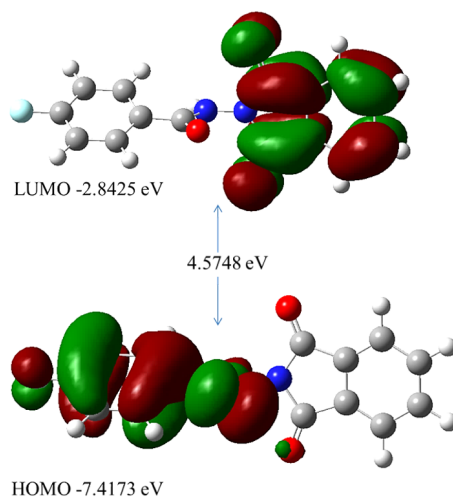


Figure 6. HOMO-LUMO diagram of compound 4.

4. Conclusions

A novel compound **4** was synthesized and thoroughly characterized using FT-IR, NMR, and HR-MS, and all of the obtained characterization data are consistent with the postulated structure. Compound **4** formed in a monoclinic system with the space group $P2_1/n$, and single crystal X-ray diffraction experiments verified its three-dimensional structure. By using DFT calculations, the obtained experimental bond angles, bond lengths, and torsion angles are in good agreement with the

theoretical values. Furthermore, DFT/B3LYP/6-311G(d,p) calculation was used to obtain some molecular properties of compound **4**. Investigating the stability, intramolecular charge transfers, donor-acceptor interactions, and strength of hydrogen bonds in the synthesized molecule is supported by DFT, Hirshfeld surface analysis, and fingerprint plots. In this study, it is demonstrated that fingerprint plots are a useful tool for aiding the identification and measurement of intermolecular interactions. These findings encourage further studies on in silico molecular docking and anticancer activities.

Acknowledgements

Dr. Ramakrishnan Elancheran thanks DST-PURSE Phase II for the financial support. Prof. Sentharamaiah Kabilan thanks The University Grants Commission, New Delhi, for the UGC BSR Faculty Fellowship.

Supporting information

CCDC-2201423 contains the supplementary crystallographic data for this paper. These data can be obtained free of charge via <https://www.ccdc.cam.ac.uk/structures/>, or by e-mailing data_request@ccdc.cam.ac.uk, or by contacting The Cambridge Crystallographic Data Centre, 12 Union Road, Cambridge CB2 1EZ, UK; fax: +44(0)1223-336033.

Disclosure statement

Conflict of interest: The authors declare that they have no conflict of interest. Ethical approval: All ethical guidelines have been adhered. Sample availability: Sample of the title compound is available from the author.

CRedit authorship contribution statement

Conceptualization: Ramakrishnan Elancheran; Methodology: Ramakrishnan Elancheran; Software: Ramakrishnan Elancheran; Validation: Balakrishnan Karthikeyan; Formal Analysis: Ramakrishnan Elancheran; Investigation: Ramakrishnan Elancheran, Balakrishnan Karthikeyan; Resources: Sentharamaiah Kabilan; Data Curation: Ramakrishnan Elancheran; Writing - Original Draft: Ramakrishnan Elancheran; Writing - Review and Editing: Balakrishnan Karthikeyan, S. Srinivasan; Visualization: S. Srinivasan; Funding acquisition: Sentharamaiah Kabilan; Supervision: Balakrishnan Karthikeyan, Kuppasamy Krishnasamy, Sentharamaiah Kabilan; Project Administration: Kuppasamy Krishnasamy, Sentharamaiah Kabilan.

ORCID and Email

Ramakrishnan Elancheran

 srielancheran@gmail.com

 <https://orcid.org/0000-0002-2819-5319>

Balakrishnan Karthikeyan

 bkarthi_au@yahoo.com

 <https://orcid.org/0000-0002-7545-1370>

Subramanian Srinivasan

 drssvasan74@rediffmail.com

 <https://orcid.org/0000-0003-0848-5236>

Kuppasamy Krishnasamy

 krishnasamybala56@gmail.com

 <https://orcid.org/0000-0001-5062-6982>

Sentharamaiah Kabilan

 profdrskabilanau@gmail.com

 <https://orcid.org/0000-0002-8060-7886>

References

- Halim, P. A.; Georgey, H. H.; George, M. Y.; El Kerdawy, A. M.; Said, M. F. Design and synthesis of novel 4-fluorobenzamide-based derivatives as promising anti-inflammatory and analgesic agents with an enhanced gastric tolerability and COX-inhibitory activity. *Bioorg. Chem.* **2021**, *115*, 105253.
- Aliabadi, A.; Mohammadi-Frarni, A.; Azizi, M.; Ahmadi, F. Design, synthesis and cytotoxicity evaluation of N-(5-benzylthio)-4H-1,2,4-triazol-3-yl)-4-fluorobenzamide derivatives as potential anticancer agents. *Pharm. Chem. J.* **2016**, *49*, 694–699.
- Klabunde, T.; Wendt, K. U.; Kadereit, D.; Brachvogel, V.; Burger, H.-J.; Herling, A. W.; Oikonomakos, N. G.; Kosmopoulou, M. N.; Schmoll, D.; Sarubbi, E.; von Roedern, E.; Schönafinger, K.; Defossa, E. Acyl ureas as human liver glycogen phosphorylase inhibitors for the treatment of type 2 diabetes. *J. Med. Chem.* **2005**, *48*, 6178–6193.
- Matalka, K. Z.; Alfarhoud, F.; Qinna, N. A.; Mallah, E. M.; Abu-Dayyih, W. A.; Muhi-elddeen, Z. A. Anti-inflammatory aminoacetylenic isoindoline-1,3-dione derivatives modulate cytokines production from different spleen cell populations. *Int. Immunopharmacol.* **2012**, *14*, 296–301.
- Kumar, S.; Kumar, N.; Roy, P.; Sondhi, S. M. Synthesis, anti-inflammatory, and antiproliferative activity evaluation of isoindole, pyrrolopyrazine, benzimidazoisindole, and benzimidazopyrrolo pyrazine derivatives. *Mol. Divers.* **2013**, *17*, 753–766.
- Bhatia, R. Isoindole derivatives: Propitious anticancer structural motifs. *Curr. Top. Med. Chem.* **2016**, *17*, 189–207.
- Tan, A.; Yaglioglu, A. S.; Kishali, N. H.; Sahin, E.; Kara, Y. Evaluation of cytotoxic potentials of some isoindole-1, 3-Dione derivatives on HeLa, C6 and A549 cancer cell lines. *Med. Chem.* **2020**, *16*, 69–77.
- Csende, F.; Porkolab, A. Antiviral activity of isoindole derivatives. *Journal of Medicinal and Chemical Sciences* **2020**, *3*, 254–285.
- Sipos, A.; Török, Z.; Róth, E.; Kiss-Szikszai, A.; Batta, G.; Bereczki, I.; Fejes, Z.; Borbás, A.; Ostorházi, E.; Rozgonyi, F.; Naesens, L.; Herczegh, P. Synthesis of isoindole and benzoisoindole derivatives of teicoplanin pseudoaglycon with remarkable antibacterial and antiviral activities. *Bioorg. Med. Chem. Lett.* **2012**, *22*, 7092–7096.
- Guzior, N.; Bajda, M.; Rakoczy, J.; Brus, B.; Gobec, S.; Malawska, B. Isoindoline-1,3-dione derivatives targeting cholinesterases: Design, synthesis and biological evaluation of potential anti-Alzheimer's agents. *Bioorg. Med. Chem.* **2015**, *23*, 1629–1637.
- Aliabadi, A.; Gholamine, B.; Karimi, T. Synthesis and antiseizure evaluation of isoindoline-1,3-dione derivatives in mice. *Med. Chem. Res.* **2014**, *23*, 2736–2743.
- Cardoso, M. V. de O.; Moreira, D. R. M.; Filho, G. B. O.; Cavalcanti, S. M. T.; Coelho, L. C. D.; Espíndola, J. W. P.; Gonzalez, L. R.; Rabello, M. M.; Hernandes, M. Z.; Ferreira, P. M. P.; Pessoa, C.; Alberto de Simone, C.; Guimarães, E. T.; Soares, M. B. P.; Leite, A. C. L. Design, synthesis and structure-activity relationship of phthalimides endowed with dual antiproliferative and immunomodulatory activities. *Eur. J. Med. Chem.* **2015**, *96*, 491–503.
- Zhen, X.; Peng, Z.; Zhao, S.; Han, Y.; Jin, Q.; Guan, L. Synthesis, potential anticonvulsant and antidepressant effects of 2-(5-methyl-2,3-dioxindolin-1-yl)acetamide derivatives. *Acta Pharm. Sin. B.* **2015**, *5*, 343–349.
- Huang, B.; Li, X.; Zhan, P.; De Clercq, E.; Daelemans, D.; Pannecouque, C.; Liu, X. Design, synthesis, and biological evaluation of novel 2-(pyridin-3-yloxy)acetamide derivatives as potential anti-HIV-1 agents. *Chem. Biol. Drug Des.* **2016**, *87*, 283–289.
- Saravanan, K.; Elancheran, R.; Divakar, S.; Kabilan, S.; Selvanayagam, S. 2-Chloro-N-(4-phenyl-1,3-thiazol-2-yl)acetamide. *IUCrdata* **2016**, *1*, x160879.
- Saravanan, K.; Divakar, S.; Elancheran, R.; Kabilan, S.; Selvanayagam, S. 4-[2-(1,3-Dioxoisindolin-2-yl)-1,3-thiazol-4-yl]benzonitrile. *IUCrdata* **2016**, *1*, x161117.
- Lakshminthendral, K.; Saravanan, K.; Elancheran, R.; Archana, K.; Manikandan, N.; Arjun, H. A.; Ramanathan, M.; Lokanath, N. K.; Kabilan, S. Design, synthesis and biological evaluation of 2-(phenoxyethyl)-5-phenyl-1,3,4-oxadiazole derivatives as anti-breast cancer agents. *Eur. J. Med. Chem.* **2019**, *168*, 1–10.
- Bruker (2016). APEX3, SAINT-Plus and SADABS. Bruker AXS Inc., Madison, Wisconsin, USA.
- Sheldrick, G. M. "SHELXS-97 and SHELXL-97, Program for Crystal Structure Solution and Refinement," University of Gottingen, Gottingen, 1997.
- Frisch, M. J.; Trucks, G. W.; Schlegel, H. B.; Scuseria, G. E.; Robb, M. A.; Cheeseman, J. R.; Scalmani, G.; Barone, V.; Mennucci, B.; Petersson, G. A.; Nakatsuji, H.; Caricato, M.; Li, X.; Hratchian, H. P.; Izmaylov, A. F.; Bloino, J.; Zheng, G.; Sonnenberg, J. L.; Hada, M.; Ehara, M.; Toyota, K.; Fukuda, R.; Hasegawa, J.; Ishida, M.; Nakajima, T.; Honda, Y.; Kitao, O.; Nakai, H.; Vreven, T.; Montgomery, J. A.; Peralta, J. E.; Ogliaro, F.; Bearpark, M.; Heyd, J. J.; Brothers, E.; Kudin, K. N.; Staroverov, V. N.; Kobayashi, R.; Normand, J.; Raghavachari, K.; Rendell, A.; Burant, J. C.; Iyengar, S. S.; Tomasi, J.; Cossi, M.; Rega, N.; Millam, J. M.; Klene, M.; Knox, J. E.; Cross, J. B.; Bakken, V.; Adamo, C.; Jaramillo, J.; Gomperts, R.; Stratmann, R. E.; Yazyev, O.; A. J. Austin, A. J.; Cammi, R.; Pomelli, C.; Ochterski, J. W.; Martin, R. L.; Morokuma, K.; Zakrzewski, V. G.; Voth, G. A.; Salvador, P.; Dannenberg, J. J.; Dapprich, S.; Daniels, A. D.; Farkas, O.; Foresman, J. B.; Ortiz, J. V.; Cioslowski, J.; Fox, D. J. Gaussian, Inc., Gaussian 09, Revision A.02, Wallingford CT, 2009.
- Becke, A. D. Density-functional thermochemistry. III. The role of exact exchange. *J. Chem. Phys.* **1993**, *98*, 5648–5652.
- Lee, C.; Yang, W.; Parr, R. G. Development of the Colle-Salvetti correlation-energy formula into a functional of the electron density. *Phys. Rev. B Condens. Matter.* **1988**, *37*, 785–789.
- Dennington, R.; Keith, T. A.; Millam, J. M. GaussView, Version 5, Semichem Inc.; Shawnee Mission, KS, 2009.
- Spackman, P. R.; Turner, M. J.; McKinnon, J. J.; Wolff, S. K.; Grimwood, D. J.; Jayatilaka, D.; Spackman, M. A. CrystalExplorer: a program for Hirshfeld surface analysis, visualization and quantitative analysis of molecular crystals. *J. Appl. Crystallogr.* **2021**, *54*, 1006–1011.
- Hirshfeld, F. L. Bonded-atom fragments for describing molecular charge densities. *Theoret. Chim. Acta* **1977**, *44*, 129–138.
- Wolff, S. K.; Grimwood, D.; McKinnon, J.; Jayatilaka, D.; Spackman, M. *Crystal Explorer 3.0*, University of Western Australia, Perth, Australia, 2012.
- Binzet, G.; Flörke, U.; Külcü, N.; Arslan, H. Crystal and molecular structure of bis(4-bromo-N-(di-n-butylcarbamothioyl)benzamido) copper(II) complex. *Eur. J. Chem.* **2012**, *3*, 211–213.

- [28]. Bülbül, H.; Köysal, Y.; Dege, N.; Gümüş, S.; Açar, E. Crystal structure, spectroscopy, SEM analysis, and computational studies of N-(1,3-dioxoisindolin-2-yl)benzamide. *J. Crystallogr.* **2015**, *2015*, 1–6.
- [29]. Etse, K. S.; Lamela, L. C.; Zaragoza, G.; Pirotte, B. Synthesis, crystal structure, Hirshfeld surface and interaction energies analysis of 5-methyl-1,3-bis(3-nitrobenzyl)pyrimidine-2,4(1H,3H)-dione. *Eur. J. Chem.* **2020**, *11*, 91–99.
- [30]. Ahangar, A. A.; Elancheran, R.; Dar, A. A. Influence of halogen substitution on crystal packing, molecular properties and electrochemical sensing. *J. Solid State Chem.* **2022**, *314*, 123382.



Copyright © 2023 by Authors. This work is published and licensed by Atlanta Publishing House LLC, Atlanta, GA, USA. The full terms of this license are available at <http://www.eurjchem.com/index.php/eurjchem/pages/view/terms> and incorporate the Creative Commons Attribution-Non Commercial (CC BY NC) (International, v4.0) License (<http://creativecommons.org/licenses/by-nc/4.0>). By accessing the work, you hereby accept the Terms. This is an open access article distributed under the terms and conditions of the CC BY NC License, which permits unrestricted non-commercial use, distribution, and reproduction in any medium, provided the original work is properly cited without any further permission from Atlanta Publishing House LLC (European Journal of Chemistry). No use, distribution, or reproduction is permitted which does not comply with these terms. Permissions for commercial use of this work beyond the scope of the License (<http://www.eurjchem.com/index.php/eurjchem/pages/view/terms>) are administered by Atlanta Publishing House LLC (European Journal of Chemistry).